$\bar{d}$ and ${}^3\overline{\text{He}}$ Production in $\sqrt{s_{NN}} = 130$ GeV Au + Au Collisions

C. Adler,[11] Z. Ahammed,[23] C. Allgower,[12] J. Amonett,[14] B. D. Anderson,[14] M. Anderson,[5] G. S. Averichev,[9] J. Balewski,[12] O. Barannikova,[9,23] L. S. Barnby,[14] J. Baudot,[13] S. Bekele,[20] V. V. Belaga,[9] R. Bellwied,[30] J. Berger,[11] H. Bichsel,[29] L. C. Bland,[12] C. O. Blyth,[3] B. E. Bonner,[24] A. Boucham,[26] A. Brandin,[18] R. V. Cadman,[1] H. Caines,[20] M. Calderón de la Barca Sánchez,[31] A. Cardenas,[23] J. Carroll,[15] J. Castillo,[26] M. Castro,[30] D. Cebra,[5] S. Chattopadhyay,[30] M. L. Chen,[2] Y. Chen,[6] S. P. Chernenko,[9] M. Cherney,[8] A. Chikanian,[31] B. Choi,[27] W. Christie,[2] J. P. Coffin,[13] T. M. Cormier,[30] J. G. Cramer,[29] H. J. Crawford,[4] M. DeMello,[24] W. S. Deng,[14] A. A. Derevschikov,[22] L. Didenko,[2] J. E. Draper,[5] V. B. Dunin,[9] J. C. Dunlop,[31] V. Eckardt,[16] L. G. Efimov,[9] V. Emelianov,[18] J. Engelage,[4] G. Eppley,[24] B. Erazmus,[26] P. Fachini,[25] V. Faine,[2] E. Finch,[31] Y. Fisyak,[2] D. Flierl,[11] K. J. Foley,[2] J. Fu,[15] N. Gagunashvili,[9] J. Gans,[31] L. Gaudichet,[26] M. Germain,[13] F. Geurts,[24] V. Ghazikhanian,[6] J. Grabski,[28] O. Grachov,[30] D. Greiner,[15] V. Grigoriev,[18] M. Guedon,[13] E. Gushin,[18] T. J. Hallman,[2] D. Hardtke,[15] J. W. Harris,[31] M. Heffner,[5] S. Heppelmann,[21] T. Herston,[23] B. Hippolyte,[13] A. Hirsch,[23] E. Hjort,[15] G. W. Hoffmann,[27] M. Horsley,[31] H. Z. Huang,[6] T. J. Humanic,[20] H. Hümmler,[16] G. Igo,[6] A. Ishihara,[27] Yu. I. Ivanshin,[10] P. Jacobs,[15] W. W. Jacobs,[12] M. Janik,[28] I. Johnson,[15] P. G. Jones,[3] E. Judd,[4] M. Kaneta,[15] M. Kaplan,[7] D. Keane,[14] A. Kisiel,[28] J. Klay,[5] S. R. Klein,[15] A. Klyachko,[12] A. S. Konstantinov,[22] L. Kotchenda,[18] A. D. Kovalenko,[9] M. Kramer,[19] P. Kravtsov,[18] K. Krueger,[1] C. Kuhn,[13] A. I. Kulikov,[9] G. J. Kunde,[31] C. L. Kunz,[7] R. Kh. Kutuev,[10] A. A. Kuznetsov,[9] L. Lakehal-Ayat,[26] J. Lamas-Valverde,[24] M. A. C. Lamont,[3] J. M. Landgraf,[2] S. Lange,[11] C. P. Lansdell,[27] B. Lasiuk,[31] F. Laue,[2] A. Lebedev,[2] T. LeCompte,[1] R. Lednický,[9] V. M. Leontiev,[22] M. J. LeVine,[2] Q. Li,[30] Q. Li,[15] S. J. Lindenbaum,[19] M. A. Lisa,[20] T. Ljubicic,[2] W. J. Llope,[24] G. LoCurto,[16] H. Long,[6] R. S. Longacre,[2] M. Lopez-Noriega,[20] W. A. Love,[2] D. Lynn,[2] R. Majka,[31] S. Margetis,[14] L. Martin,[26] J. Marx,[15] H. S. Matis,[15] Yu. A. Matulenko,[22] T. S. McShane,[8] F. Meissner,[15] Yu. Melnick,[22] A. Meschanin,[22] M. Messer,[2] M. L. Miller,[31] Z. Milosevich,[7] N. G. Minaev,[22] J. Mitchell,[24] V. A. Moiseenko,[10] D. Moltz,[15] C. F. Moore,[27] V. Morozov,[15] M. M. de Moura,[30] M. G. Munhoz,[25] G. S. Mutchler,[24] J. M. Nelson,[3] P. Nevski,[2] V. A. Nikitin,[10] L. V. Nogach,[22] B. Norman,[14] S. B. Nurushev,[22] G. Odyniec,[15] A. Ogawa,[21] V. Okorokov,[18] M. Oldenburg,[16] D. Olson,[15] G. Paic,[20] S. U. Pandey,[30] Y. Panebratsev,[9] S. Y. Panitkin,[2] A. I. Pavlinov,[30] T. Pawlak,[28] V. Perevoztchikov,[2] W. Peryt,[28] V. A. Petrov,[10] E. Platner,[24] J. Pluta,[28] N. Porile,[23] J. Porter,[2] A. M. Poskanzer,[15] E. Potrebenikova,[9] D. Prindle,[29] C. Pruneau,[30] S. Radomski,[28] G. Rai,[15] O. Ravel,[26] R. L. Ray,[27] S. V. Razin,[9,12] D. Reichhold,[8] J. G. Reid,[29] F. Retiere,[15] A. Ridiger,[18] H. G. Ritter,[15] J. B. Roberts,[24] O. V. Rogachevski,[9] J. L. Romero,[5] C. Roy,[26] D. Russ,[7] V. Rykov,[30] I. Sakrejda,[15] J. Sandweiss,[31] A. C. Saulys,[2] I. Savin,[10] J. Schambach,[27] R. P. Scharenberg,[23] N. Schmitz,[16] L. S. Schroeder,[15] A. Schüttauf,[16] K. Schweda,[15] J. Seger,[8] D. Seliverstov,[18] P. Seyboth,[16] E. Shahaliev,[9] K. E. Shestermanov,[22] S. S. Shimanskii,[9] V. S. Shvetcov,[10] G. Skoro,[9] N. Smirnov,[31] R. Snellings,[15] J. Sowinski,[12] H. M. Spinka,[1] B. Srivastava,[23] E. J. Stephenson,[12] R. Stock,[11] A. Stolpovsky,[30] M. Strikhanov,[18] B. Stringfellow,[23] C. Struck,[11] A. A. P. Suaide,[30] E. Sugarbaker,[20] C. Suire,[13] M. Šumbera,[9] T. J. M. Symons,[15] A. Szanto de Toledo,[25] P. Szarwas,[28] J. Takahashi,[25] A. H. Tang,[14] J. H. Thomas,[15] V. Tikhomirov,[18] T. A. Trainor,[29] S. Trentalange,[6] M. Tokarev,[9] M. B. Tonjes,[17] V. Trofimov,[18] O. Tsai,[6] K. Turner,[2] T. Ullrich,[2] D. G. Underwood,[1] G. Van Buren,[2] , A. M. VanderMolen,[17] A. Vanyashin,[15] I. M. Vasilevski,[10] A. N. Vasiliev,[22] S. E. Vigdor,[12] S. A. Voloshin,[30] F. Wang,[23] H. Ward,[27] J. W. Watson,[14] R. Wells,[20] T. Wenaus,[2] G. D. Westfall,[17] C. Whitten, Jr.,[6] H. Wieman,[15] R. Willson,[20] S. W. Wissink,[12] R. Witt,[14] N. Xu,[15] Z. Xu,[31] A. E. Yakutin,[22] E. Yamamoto,[6] J. Yang,[6] P. Yepes,[24] A. Yokosawa,[1] V. I. Yurevich,[9] Y. V. Zanevski,[9] I. Zborovský,[9] H. Zhang,[31] W. M. Zhang,[14] R. Zoulkarneev,[10] and A. N. Zubarev[9]

(STAR Collaboration)

[1]*Argonne National Laboratory, Argonne, Illinois 60439*
[2]*Brookhaven National Laboratory, Upton, New York 11973*
[3]*University of Birmingham, Birmingham, United Kingdom*
[4]*University of California, Berkeley, California 94720*
[5]*University of California, Davis, California 95616*
[6]*University of California, Los Angeles, California 90095*
[7]*Carnegie Mellon University, Pittsburgh, Pennsylvania 15213*
[8]*Creighton University, Omaha, Nebraska 68178*
[9]*Laboratory for High Energy (JINR), Dubna, Russia*
[10]*Particle Physics Laboratory (JINR), Dubna, Russia*
[11]*University of Frankfurt, Frankfurt, Germany*

[12]Indiana University, Bloomington, Indiana 47408
[13]Institut de Recherches Subatomiques, Strasbourg, France
[14]Kent State University, Kent, Ohio 44242
[15]Lawrence Berkeley National Laboratory, Berkeley, California 94720
[16]Max-Planck-Institut für Physik, Munich, Germany
[17]Michigan State University, East Lansing, Michigan 48824
[18]Moscow Engineering Physics Institute, Moscow, Russia
[19]City College of New York, New York City, New York 10031
[20]Ohio State University, Columbus, Ohio 43210
[21]Pennsylvania State University, University Park, Pennsylvania 16802
[22]Institute of High Energy Physics, Protvino, Russia
[23]Purdue University, West Lafayette, Indiana 47907
[24]Rice University, Houston, Texas 77251
[25]Universidade de Sao Paulo, Sao Paulo, Brazil
[26]SUBATECH, Nantes, France
[27]University of Texas, Austin, Texas 78712
[28]Warsaw University of Technology, Warsaw, Poland
[29]University of Washington, Seattle, Washington 98195
[30]Wayne State University, Detroit, Michigan 48201
[31]Yale University, New Haven, Connecticut 06520
(Received 20 August 2001; published 7 December 2001)

The first measurements of light antinucleus production in Au + Au collisions at the Relativistic Heavy-Ion Collider are reported. The observed production rates for $\bar{d}$ and $^3\overline{\text{He}}$ are much larger than in lower energy nucleus-nucleus collisions. A coalescence model analysis of the yields indicates that there is little or no increase in the antinucleon freeze-out volume compared to collisions at CERN SPS energy. These analyses also indicate that the $^3\overline{\text{He}}$ freeze-out volume is smaller than the $\bar{d}$ freeze-out volume.

DOI: 10.1103/PhysRevLett.87.262301 PACS numbers: 25.75.Dw

The Relativistic Heavy-Ion Collider (RHIC) at Brookhaven National Laboratory (BNL) has recently begun operation with Au beams at $\sqrt{s_{NN}} = 130$ GeV and extend the available center-of-mass energy in nucleus-nucleus collisions by nearly a factor of 8 over CERN Super Proton Synchrotron (SPS) collisions at $\sqrt{s_{NN}} = 17$ GeV. First measurements from RHIC indicate an increase of at least 70% in the charged multiplicity for central collisions compared to previous measurements [1]. Measurements of the antiproton-to-proton ratio at midrapidity [2] indicate that the central collision region is approaching the net-baryon free limit. Such a system with large multiplicity and small net-baryon density is well suited for the production of light antinuclei. In this Letter, we report the first measurements of $\bar{d}$ and $^3\overline{\text{He}}$ production at RHIC.

At RHIC energies, production of antinuclei is possible via two mechanisms. The first mechanism is direct production of nucleus-antinucleus pairs in elementary nucleon-nucleon or parton-parton interactions. Because of their small binding energies, nuclei or antinuclei produced via early direct production are likely to be dissociated in the medium before escaping.

The second, and presumably dominant, mechanism for antinucleus production is via final-state coalescence [3–5]. In this picture, produced antinucleons merge to form light antinuclear clusters during the final stages of kinetic freeze-out. The measured yield of nuclei or antinuclei with nucleon number A and momentum P is related to the primordial nucleon invariant yield at momentum $p = P/A$ through a coalescence parameter B_A,

$$E\,\frac{d^3N_A}{d^3P} = B_A\left(E\,\frac{d^3N_N}{d^3p}\right)^A. \qquad (1)$$

Equation (1) requires that antineutrons and antiprotons be produced with identical momentum spectra.

Previous studies of smaller collision systems have noted that the measured coalescence parameter B_A can be directly predicted from the nuclear wave function of the produced (anti)nucleus [3]. When going to higher energies or larger collision systems, however, the measured coalescence parameter is lower than that measured in small systems. This can be understood by noting that once the collision region is larger than the intrinsic size of the produced (anti)nucleus, (anti)nucleons of equal velocity are not always in close proximity and hence do not always form a bound state [6]. The coalescence parameter can be used to infer the space-time geometry of the system [7]. Measurements of light nuclei and antinuclei are thus analogous to two-particle Hanbury-Brown-Twiss (HBT) correlations in that they measure "homogeneity lengths" of the system at kinetic freeze-out [8].

The measurements were made using the STAR detector [9]. The main tracking detector is a cylindrical Time-Projection Chamber (TPC) inside a 0.25 T solenoidal magnet. The TPC tracks and identifies most charged particles produced in the central pseudorapidity region ($-1.8 < \eta < 1.8$) with nearly full azimuthal coverage.

Events are selected on the basis of coincidence of spectator neutron signals in two zero-degree calorimeters located ± 18.25 m from the nominal interaction region. Central events are selected using a central trigger barrel that measures the charged-particle multiplicity with full azimuthal coverage in the pseudorapidity region $-1 < \eta < 1$. This analysis focuses on semicentral events, where the centrality corresponds to roughly the most central 18% of the measured minimum-bias multiplicity distribution. The analysis uses $\approx$600 000 events, where the interaction vertex is within the range covered by the TPC ($-200 < z < 200$ cm).

Particle identification is done by measuring the average ionization energy loss (dE/dx) for each track. The STAR electronics show no evidence for saturation below 30 times minimum ionizing. For the tracks used in this analysis, the dE/dx resolution is $\approx$11%. For each track, up to 45 ionization space-point samples are taken along the path through the TPC. Space points are found by identifying local maxima of the analog-to-digital converter (ADC) distribution. Merged ionization clusters, where multiple tracks contribute, are identified by looking for multipeaked structure in the ADC distribution. For the current analysis of relatively rare particles, it is necessary to impose tight cuts to eliminate background tracks with improperly measured dE/dx. We require a track to have at least 35 of the 45 possible space points. For central events, cluster merging is quite common and can lead to problems with the particle identification. To avoid these problems, we eliminate potentially merged clusters from the sample used to calculate the dE/dx. We require that no more than 30% of the measured space points come from potentially merged clusters. To avoid the Landau tails in the dE/dx spectrum, we use a truncated mean of the lowest 70% of the measured dE/dx samples. Figure 1 shows the measured truncated mean dE/dx versus the magnetic rigidity for the negatively charged tracks considered in this analysis.

Figure 1 also shows the Bethe-Bloch expectation for $\bar{d}$, $\bar{t}$, and $^3\overline{\mathrm{He}}$. There is a clear $\bar{d}$ band below rigidity $\approx$1 GeV/c. This analysis uses only the kinematic region of good $\bar{d}$ particle identification and efficiency ($0.5 < p_T < 0.8$ GeV/c and rapidity $|y| < 0.3$). We observe 14 counts clustered around the $^3\overline{\mathrm{He}}$ expectation in the kinematic range $1.0 < p_T < 5.0$ GeV/c and $|y| < 0.8$. Note that we plot the rigidity, so the momentum of the $^3\overline{\mathrm{He}}$ candidates is twice as large. No clear $\bar{t}$ band is observed, but if one assumes that $\bar{t}$ and $^3\overline{\mathrm{He}}$ are produced in similar numbers and with similar momentum distributions we would expect the bulk of the $\bar{t}$ to have a higher rigidity where our dE/dx resolution is inadequate for their identification.

To extract the $\bar{d}$ yield, we construct a quantity $Z = \log\{[dE/dx]/I_{\bar{d}}(p)\}$, where $I_{\bar{d}}(p)$ is the expected ionization for a $\bar{d}$ of momentum p. For a pure sample of $\bar{d}$, this quantity should be well described by a Gaussian centered at zero. In the inset of Fig. 1, we plot the Z distribution for one transverse momentum bin. We see a Gaussian $\bar{d}$ signal superimposed upon a background due to the tail of the $\bar{p}$ distribution. We parametrize the $\bar{p}$ background in the tail region as an exponential, and fit the resulting distribution to a Gaussian $\bar{d}$ signal plus exponential $\bar{p}$ tail hypothesis. In the inset of Fig. 1, we also show (by the curve) our exponential plus Gaussian fit. In the $\bar{d}$ kinematic region considered, the signal-to-background ratio ranges from 30 in the lowest p_T bin to 3 in the highest p_T bin. We performed a similar analysis of the $^3\overline{\mathrm{He}}$ Z distribution, and estimated the total background to be less than 0.5 counts.

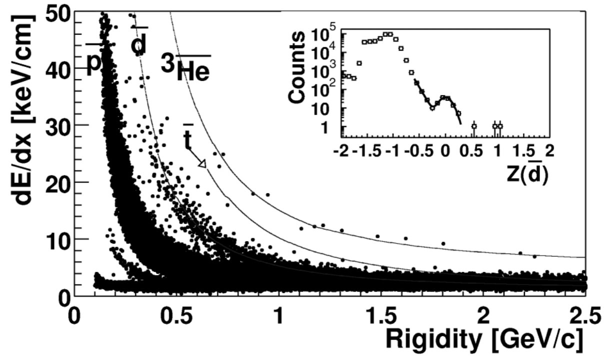

FIG. 1. Ionization (dE/dx) versus rigidity (|momentum/nuclear charge units|) for negative tracks. The π^- and K^- bands have been suppressed. Also plotted are the Bethe-Bloch expectations for $\bar{d}$, $\bar{t}$, and $^3\overline{\mathrm{He}}$. The inset shows a projection of the Z variable (see text) for one transverse momentum bin ($0.6 < p_T < 0.7$ GeV/c, $|y| < 0.3$).

To evaluate the efficiency, we use GEANT and a TPC response simulator to create raw pixel level simulated tracks which we then embed into real events. The embedding is crucial for this analysis since it allows us to estimate the effects of cluster merging on our efficiency. No data on $\bar{d}$ and $^3\overline{\mathrm{He}}$ interactions in material exist in the literature, and these antinuclei are not incorporated into GEANT. Instead we use d and ^{3}He simulations in GEANT to understand our acceptance and tracking efficiency. We then add a correction for the estimated annihilation in the detector, where we assume that the $\bar{d}$ annihilation cross section is 1.4 times the $\bar{p}$ annihilation cross section, and that the $^3\overline{\mathrm{He}}$ annihilation cross section is twice the $\bar{p}$ annihilation cross section. The $\bar{p}$ annihilation correction was discussed in a previous publication [2], and the cross-section scaling relations are taken from Ref. [10]. Final calculated efficiencies are in the range 0.2–0.5. This is much lower than the typical STAR efficiency for charged particle tracking (0.8–0.9). The difference is due entirely to the restrictive track cuts used in the current analysis to eliminate backgrounds.

Systematic errors were estimated by varying the cuts used in the analysis. These variations include changing the number of hits for a valid track, changing the allowed region of vertex locations, changing the assumed annihilation cross sections, and changing the Z range used for the signal plus background fit. We estimate the maximum systematic error on the invariant yields to be about 15%. We also assume that the errors on the individual yields are largely correlated. This causes the systematic errors to partially cancel when forming coalescence ratios.

TABLE I. Measured invariant yields of antinuclei. The errors quoted are statistical only. Systematic errors are estimated to be 15%. Also listed are $\bar{p}$ invariant yields at the same velocity, and the weak-decay correction to the $\bar{p}$ yield estimated from RQMD.

	p_T (GeV/c)	$E\frac{d^3N}{d^3p}$ (GeV^{-2} c^3)	$\bar{p}$ $E\frac{d^3N}{d^3(p/A)}$ (GeV^{-2} c^3)	Weak-decay correction
	0.55	$[2.47 \pm 0.26] \times 10^{-3}$	4.20 ± 0.12	0.56
$\bar{d}$	0.65	$[1.87 \pm 0.19] \times 10^{-3}$	4.00 ± 0.10	0.53
	0.75	$[1.93 \pm 0.20] \times 10^{-3}$	3.82 ± 0.09	0.52
$^3\overline{\mathrm{He}}$	2.4	$[8.4 \pm 2.3] \times 10^{-7}$	2.63 ± 0.04	0.61

We extract $\bar{d}$ invariant yields in three transverse momentum bins, where each bin has $\approx$100 entries. The extracted yields are listed in Table I. Comparing these yields to lower energies, there is a factor of $\approx$50 increase in the $\bar{d}$ production rate in going from $\sqrt{s_{NN}} = 17$ GeV [11] to $\sqrt{s_{NN}} = 130$ GeV, and an even more dramatic factor of $\approx$60 000 increase in the $\bar{d}$ production rate relative to Alternating Gradient Synchrotron (AGS) (at BNL) energy ($\sqrt{s_{NN}} = 4.9$ GeV) [12].

The mean transverse momentum of the observed $^3\overline{\mathrm{He}}$ sample is ≈ 2.4 GeV$/c$. We extract an invariant yield per event evaluated at the mean p_T of $[8.4 \pm 2.3(\mathrm{stat}) \pm 1.3(\mathrm{syst})] \times 10^{-7}$ GeV^{-2} c^3. NA52 has reported two $^3\overline{\mathrm{He}}$ in minimum-bias Pb + Pb collisions at the CERN SPS [14]. Our invariant yield is higher, but quantitative comparison cannot be made because of the different centralities.

Although only 14 counts were observed, our large kinematic coverage for $^3\overline{\mathrm{He}}$ allows us to estimate the dN/dy and inverse slope T. To do this, we have calculated the expected yield as a function of y and p_T using efficiency calculations from embedded data and assuming an exponential transverse mass distribution. We minimize the negative log-likelihood over the entire STAR acceptance taking into account phase-space cells with no observed counts. We extract $^3\overline{\mathrm{He}}$ $dN/dy = [5.1 \pm 1.7(\mathrm{stat}) \pm 0.8(\mathrm{syst})] \times 10^{-5}$ and an inverse slope $T = 0.70 \pm 0.25(\mathrm{stat})$ GeV.

STAR has measured invariant yields for $\bar{p}$ in a similar centrality range [15]. These results can be combined with the invariant yields presented in this paper to calculate coalescence factors using Eq. (1). In the coalescence picture, only antinucleons produced directly from the source are available to form light antinuclei. Hence, the $\bar{p}$ yields in the coalescence ratio have been corrected for antihyperon feed-down. We use the RQMD model [16] and a detector simulator to evaluate the probability of incorrectly assigning a weak-decay produced $\bar{p}$ to the primary vertex, and find that about 45 ± 5(syst)% of our $\bar{p}$ sample comes from antihyperon feed-down. This fraction is consistent with preliminary STAR measurements of the $\bar{\Lambda}/\bar{p}$ ratio. Table I lists the total $\bar{p}$ invariant yields along with the estimated correction for antihyperon feed-down.

For the topmost 18% central collisions, we find $\langle B_2 \rangle = [4.5 \pm 0.3(\mathrm{stat}) \pm 1.0(\mathrm{syst})] \times 10^{-4}$ GeV$^2/c^3$ in the $\bar{d}$ kinematic region $0.5 < p_T < 0.8$ GeV$/c$ and $|y| < 0.3$. In the top panel of Fig. 2 we compare this result to previous measurements at lower energies. In pA collisions, B_2 is essentially independent of the collision energy. In central nucleus-nucleus collisions, however, the coalescence factor B_2 decreases as the collision energy increases from Bevalac to AGS to SPS. The STAR result shows that there is no similar decrease in B_2 from $\sqrt{s_{NN}} = 17$ GeV to $\sqrt{s_{NN}} = 130$ GeV. Comparing the STAR result to the average of the two $\bar{d}$ results at the SPS [11,14], we obtain $B_2(\mathrm{SPS})/B_2(\mathrm{RHIC}) = 1.1 \pm 0.1(\mathrm{stat})$.

For the topmost 18% most central collisions, we find $\langle B_3 \rangle = [2.1 \pm 0.6(\mathrm{stat}) \pm 0.6(\mathrm{syst})] \times 10^{-7}$ GeV$^4/c^6$ in the $^3\overline{\mathrm{He}}$ kinematic region $1.0 < p_T < 5.0$ GeV$/c$ and $|y| < 0.8$. We compare this to collisions at lower energies in the bottom panel of Fig. 2. The qualitative trend for B_3 is very similar to B_2. For pA collisions, the coalescence factor is independent of energy. For AA collisions, the coalescence factor decreases with increasing collision

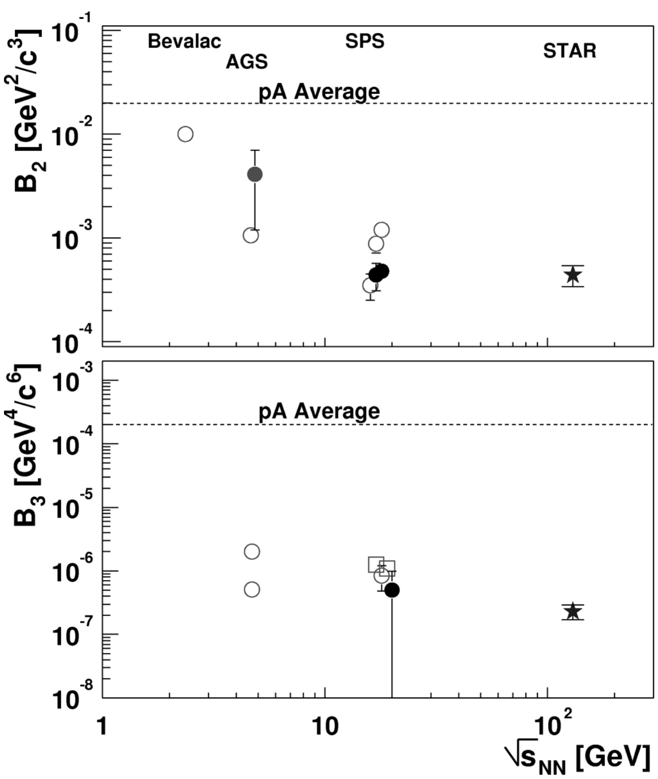

FIG. 2. Coalescence parameters B_2 and B_3 excitation functions for semicentral Au + Au or Pb + Pb collisions [11–14,17–20]. The nuclei are plotted using hollow markers, and the antinuclei are plotted using solid markers. The errors on the STAR data points are statistical (narrow bars) and systematic (wide bars).

energy. The statistics of the $^3\overline{\rm He}$ measurement at the SPS preclude a quantitative comparison. If we compare to the average of $^3\overline{\rm He}$ and ^{3}He at the SPS [14], we obtain $B_3(\mathrm{SPS})/B_3(\mathrm{RHIC}) = 3.4 \pm 1.5(\mathrm{stat})$.

Several prescriptions have been proposed for relating the coalescence parameters to a geometrical source size [6–8]. For these models, the coalescence parameter scales with the volume as $B_A \propto 1/V^{(A-1)}$ in the limit of an (anti)nucleon volume much larger than the intrinsic size of the produced (anti)nucleus. Using this simple expression, and the measured coalescence parameter ratios, we find that $V_{\bar{d}}(\mathrm{RHIC}) = (1.1 \pm 0.1)V_{\bar{d}}(\mathrm{SPS})$ and $V_{^3\overline{\rm He}}(\mathrm{RHIC}) = (1.8 \pm 0.4)V_{^3\overline{\rm He}}(\mathrm{SPS})$. Both measurements indicate no large increase of the antinucleon freeze-out volume when going from $\sqrt{s_{NN}} = 17$ GeV to $\sqrt{s_{NN}} = 130$ GeV. STAR also measured source sizes using $\pi^-\pi^-$ interferometry [21]. If we construct a quantity proportional to the volume, $V_{\pi\pi} \propto R_s^2 R_L$, and compare to the published SPS data [22], we estimate $V_{\pi^-\pi^-}(\mathrm{RHIC}) = (1.8 \pm 0.7)V_{\pi^-\pi^-}(\mathrm{SPS})$. All three available measurements indicate only a slight increase in volume compared to lower energy collisions. Caution should be exercised, however, when making quantitative comparisons between the volumes measured via coalescence and the volumes measured via HBT since it is not clear that the freeze-out space-time geometry for pions and antinucleons should be the same.

We can also make quantitive estimates of the freeze-out geometry within the context of particular coalescence models and ask whether the $\bar{d}$ and $^3\overline{\rm He}$ sources are the same. A simple thermal model [7], which assumes that antinucleons and antinuclei are in chemical and thermal equilibrium within a volume V, gives $V_{\bar{d}}/V_{^3\overline{\rm He}} = 1.8 \pm 0.3$. The Sato and Yazaki model [6] indicates a similar trend as the thermal model, with $V_{\bar{d}}/V_{^3\overline{\rm He}} = 2.2 \pm 0.3$, while the Scheibl and Heinz model [8], which can be calculated assuming a Gaussian antinucleon density profile and explicitly includes the effects of radial flow, gives $V_{\bar{d}}^{\rm eff}/V_{^3\overline{\rm He}}^{\rm eff} = 0.9 \pm 0.1$. In the Scheibl and Heinz model, an equivalent effective volume, as indicated by the data, would imply a larger total volume for $\bar{d}$ compared to $^3\overline{\rm He}$. In all models, the $^3\overline{\rm He}$ freeze-out from a smaller volume and at a presumably earlier time compared to $\bar{d}$. This trend of decreasing source size with increasing nucleon number has been observed previously in the production of light nuclei [7,12]. The coalescence picture of light antinucleus production would predict that the probability for producing an antinucleus with mass A is proportional to the Ath power of the *local* antinucleon density. If the antinucleon source is not of uniform density, one would expect the different mass antinuclei to measure different source sizes, and this is indeed what we observe.

In summary, we have made the first measurements of the production of light antinuclei ($\bar{d}$ and $^3\overline{\rm He}$) in Au + Au collisions at $\sqrt{s_{NN}} = 130$ GeV. A large enhancement in production rate is observed compared to lower energies. We have combined the measured yields with measurements of $\bar{p}$ production to extract coalescence parameters B_2 and B_3. Quantitative comparisons to SPS results indicate little or no increase of the antinucleon freeze-out volume. We also find that the $^3\overline{\rm He}$ are produced from a smaller volume than the $\bar{d}$.

We wish to thank the RHIC Operations Group and the RHIC Computing Facility at Brookhaven National Laboratory, and the National Energy Research Scientific Computing Center at Lawrence Berkeley National Laboratory for their support. This work was supported by the Division of Nuclear Physics and the Division of High Energy Physics of the Office of Science of the U.S. Department of Energy, the United States National Science Foundation, the Bundesministerium fuer Bildung und Forschung of Germany, the Institut National de la Physique Nucleaire et de la Physique des Particules of France, the United Kingdom Engineering and Physical Sciences Research Council, Fundacao de Amparo a Pesquisa do Estado de Sao Paulo, Brazil, and the Russian Ministry of Science and Technology.

[1] Phobos Collaboration, B. B. Back *et al.,* Phys. Rev. Lett. **85**, 3100 (2000).
[2] STAR Collaboration, C. Adler *et al.,* Phys. Rev. Lett. **86**, 4778 (2001).
[3] S. T. Butler and C. A. Pearson, Phys. Rev. **129**, 836 (1963).
[4] A. Schwarzschild and C. Zupancic, Phys. Rev. **129**, 854 (1963).
[5] H. H. Gutbrod *et al.,* Phys. Rev. Lett. **37**, 667 (1976).
[6] H. Sato and K. Yazaki, Phys. Lett. **98B**, 153 (1981).
[7] A. Z. Mekjian, Phys. Rev. C **17**, 1051 (1978); S. Das Gupta and A. Z. Mekjian, Phys. Rep. **72**, 131 (1981).
[8] R. Scheibl and U. Heinz, Phys. Rev. C **59**, 1585 (1999).
[9] K. H. Ackermann *et al.,* Nucl. Phys. **A661**, 681c (1999).
[10] T. F. Hoang, Bruce Cork, and H. J. Crawford, Z. Phys. C **29**, 611 (1985).
[11] NA44 Collaboration, I. G. Bearden *et al.,* Phys. Rev. Lett. **85**, 2681 (2000).
[12] E864 Collaboration, T. A. Armstrong *et al.,* Phys. Rev. Lett. **85**, 2685 (2000); E864 Collaboration, T. A. Armstrong *et al.,* Phys. Rev. C **61**, 064908 (2000).
[13] EOS Collaboration, S. Wang *et al.,* Phys. Rev. Lett. **74**, 2646 (1995).
[14] NA52 Collaboration, G. Appelquist *et al.,* Phys. Lett. B **376**, 245 (1996); NA52 Collaboration, M. Weber *et al.,* Nucl. Phys. **A661**, 177c (1999).
[15] STAR Collaboration, C. Adler *et al.,* following Letter, Phys. Rev. Lett. **87**, 262302 (2001).
[16] H. Sorge, Phys. Rev. C **52**, 3291 (1995).
[17] NA52 Collaboration, G. Ambrosini *et al.,* Phys. Lett. B **417**, 202 (1998).
[18] NA44 Collaboration, A. G. Hansen *et al.,* Nucl. Phys. **A661**, 387c (1999).
[19] NA49 Collaboration, S. V. Afanasiev *et al.,* Phys. Lett. B **486**, 22 (2000).
[20] E878 Collaboration, M. J. Bennett *et al.,* Phys. Rev. C **58**, 1155 (1998).

[21] STAR Collaboration, C. Adler *et al.,* Phys. Rev. Lett. **87**, 082301 (2001).

[22] NA44 Collaboration, I. G. Bearden *et al.,* Phys. Rev. C **58**, 1656 (1998).